


Article

# Design and Experimental Evaluation of a Low-Cost Test Rig for Flywheel Energy Storage Burst Containment Investigation

Armin Buchroithner \*, Peter Haidl, Christof Birgel, Thomas Zarl and Hannes Wegleiter<sup>ID</sup>

Institute of Electrical Measurement and Measurement Signal Processing, Graz University of Technology, 8010 Graz, Austria; haidl@tugraz.at (P.H.); c.birgel@student.tugraz.at (C.B.); t.zarl@student.tugraz.at (T.Z.); wegleiter@tugraz.at (H.W.)

\* Correspondence: armin.buchroithner@tugraz.at; Tel.: +43-316-873-30514

Received: 30 October 2018; Accepted: 11 December 2018; Published: 14 December 2018



**Featured Application:** This article covers the design and operation of a low-cost test rig as a strategic tool to aid the development of burst containments for flywheel energy storage systems.

**Abstract:** Data related to the performance of burst containments for high-speed rotating machines, such as flywheel energy storage systems (FESS), turbines or electric motors is scarce. However, development of optimized burst containment structures requires statistically significant data, which calls out for low-cost test methods as a strategic development tool. Consequently, a low-cost test rig (so called spin pit) for the investigation of burst containments was designed, with the goal to systematically investigate the performance of different containment structures and materials, in conjunction with the failure mechanisms of different rotors. The gathered data (e.g., burst speed, acceleration, temperature, ambient pressure, etc.) in combination with a post-mortem analysis was used to draw an energy balance and enabled the assessment of the effectiveness of various burst containments.

**Keywords:** flywheel energy storage; burst containment; high-speed rotating machines; spin pit; spin testing; test rig design

## 1. Introduction

Motor downsizing and rotor up-speeding can be observed as a general trend in many applications of engineering, in fields ranging from electric mobility to turbo machinery. Rotors are increasingly being operated at extremely high rim speeds in order to fully exploit material strength and allow light-weight engineering. This trend, however, results in severe centripetal stresses and a potential safety threat in case of rotor failure. Another example, in which high speed rotors play an important role, are flywheel energy storage systems (FESS), where the stored kinetic energy is a function of the rotor speed squared. Compared to chemical energy storage (e.g., batteries) FESS can reach extremely high cycle life because of the absence of chemical aging. This unique property, in combination with high specific power, has caused this millennia-old energy storage principle to experience a renaissance due to its suitability to store renewable energy [1], improve grid stability [2], and recuperate braking energy in (hybrid-)vehicles [3,4]. Even though there are many different architectures of FESS the most common topology—a non-integrated electromechanical system is sketched out in Figure 1 to illustrate how this energy storage principle works.

In order to gain high specific energy contents in FESS, rotor speeds must be increased (compare Formula (1) in Section 2.1) and the strength of the rotor material must be fully exploited by operating at

highest permissible centripetal stress. In this context, burst containments/housings are safety-critical parts and, even if reliable numerical methods were available, the designs need to be validated via experimental tests. However, empirical investigation (so called ‘burst’ or ‘over-speed tests’) of rotors in conjunction with the respective burst containments require significant financial and engineering effort (compare Section 3.2). This is why—if at all—usually only one single test is performed to validate one specific rotor-containment combination.

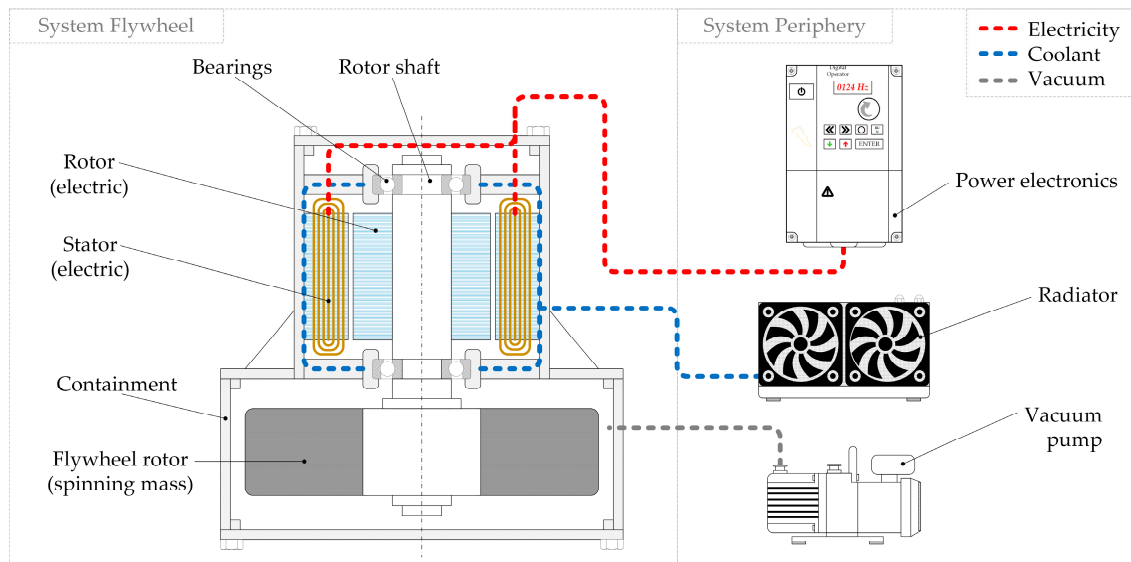


**Figure 1.** Typical layout of a non-integrated electromechanical flywheel energy storage system (FESS) [5].

Data related to the performance of burst containments for high-speed rotating machinery—such as flywheels, turbines, or electric motors—is scarce because the developers usually consider it a company secret. Never the less, optimized development of burst containment structures requires statistically significant data, which stresses the importance of low-cost test methods as a strategic development tool. Consequently, a small-scale, low-cost test rig for the investigation of burst containments was designed with the goal to investigate the performance of different containment structures and materials, as well as the failure mechanisms and interactions with different rotors. The gathered data (i.e., burst speed, acceleration, temperature, ambient pressure, etc.) in combination with a post-mortem analysis (as presented in Section 5) was used to draw an energy balance and hence allows for the assessment of the effectiveness of the burst containment.

## 2. Burst Containments for FESS

While flywheel energy storage is not inherently dangerous, significant design errors may lead to malfunctions or in the worst case even rotor burst. Even though there are hardly any known FESS accidents, which caused personal injuries, rare incidents like the rotor crash at the Beacon Power Grid Stability Plant [6] are enough to make society (and more importantly investors) suspicious [7]. So far, only few accidents, in which the FESS burst containment was penetrated, have been mentioned in literature. Two prominent examples, also shown in Figure 2a,b, are:

- 2011, Beacon Power: Crash of a 1-ton, 30 kWh carbon and glass composite rotor.
- 2015, Quantum Technologies: Failure of a 5-ton, 100 kWh steel rotor.

Any other information on FESS housing failure available in literature is related to rotors deliberately destroyed during burst tests (compare Section 3.1). However, it must be clearly distinguished between isotropic (mainly steel) rotors and anisotropic (fiber-composite) rotors, since their burst behavior is significantly different, as will also be discussed in Section 3.





**Figure 2.** (a) Impressions of the accidents at Beacon Power in Stephentown [8]; (b) Quantum Technologies flywheel-plant in San Diego, USA [9].

### 2.1. Energy Storage Capabilities of Rotor Materials

In order to optimally design FESS burst containments it is important to fully understand how energy is actually stored in the rotor. As described in Equation (1), the kinetic energy is proportional to the rotor's moment of inertia,  $I$ , and the rotational speed,  $\omega$ , squared.

$$E_k = \frac{1}{2} I \omega^2 \quad (1)$$

The maximum *kinetic energy*  $E_{k\_max}$  that can be stored in the flywheel is limited by the maximum admissible centripetal stresses,  $\sigma_{max}$ , which occur in the rotor and can be described as

$$E_{k\_max} = K_{shape} \frac{\sigma_{max}}{\rho} \quad (2)$$

$K_{shape}$  is the so-called shape factor, a geometric design variable ranging from 0.3 to 1 depending on rotor geometry [10]. Hence, from a material point of view, the function of  $\sigma/\rho$  (the ratio between tensile strength and rotor material density) determines the storable specific energy, indicating that light, yet strong materials hold the greatest potential. At the current state of the art and under consideration of a safety factor of 2 (50% exploitation of the rotor material) 31 kg of high-strength steel or 7 kg of high-strength carbon fiber composite (*TG1000*) are required to store 1 kWh of energy. Still, as long as there are advances in material science, the specific energies (and energy densities) of FESS will increase further over time. Though only expected in the distant future, flywheel rotors made of carbon nano-tube technology could result in a radical change in the energy storage sector, revealing a theoretical potential of up to 15 kWh/kg [5]. A comparison of FESS rotors with fossil fuels, which offer an energy density of ~12 kWh/kg and Li-Ion batteries (at ~0.25 kWh/kg) is given in Figure 3.

It must be stressed that the performance of FESS safety housings needs to increase at the same rate as the specific energy content of rotors does! This is not only important in order to guarantee perfect safety of this energy storage technology, but also to allow full exploitation of both the rotor and housing material, as described in the subsequent section.

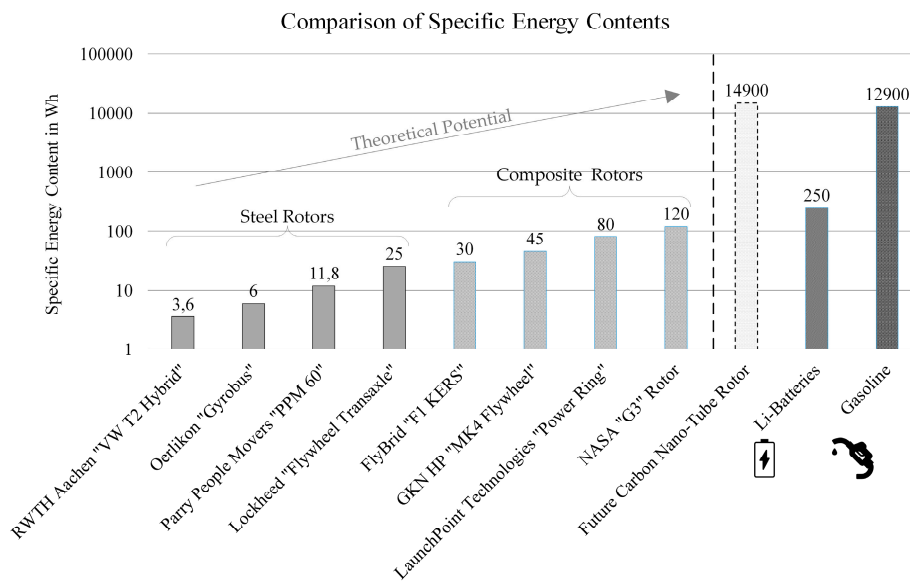


**Figure 3.** Comparison of specific energy content of existing FESS rotors and possible future carbon nanotube rotor with Li-Ion batteries and fossil fuels. Please also note the logarithmic scale.

## 2.2. Requirements for FESS Burst Containments

The FESS-housing is a part, which mainly has to fulfill the following three tasks:

1. Interface between moving (rotating) parts and the stationary environment
2. Provision of air tightness for a vacuum rotor atmosphere
3. Protection against rupture of rotor debris during possible failure or vehicle crash

Figure 4 shows the eight most relevant aspects of FESS housing design, which were identified in [11]. Besides the aspect of safety (which always needs to be attributed with highest priority), image (appearance) and cost, the FESS housing design must be carried out considering the following criteria:

- Light weight: The high specific (kinetic) energy of the FESS-rotor is reduced to a fraction at system level, mainly due to the high weight of the housing.
- Desired machine dynamics: Positive influence on rotor dynamics and acoustics due to housing structure and material properties is required (e.g., specific stiffness and damping).
- Suitability for cooling system: A proper cooling circuit for electric motor-generator and bearing system must be easily integrated in the housing.
- Low cost: Low-cost materials and efficient manufacturing processes (suitable for serial production) must be selected for the burst containment.

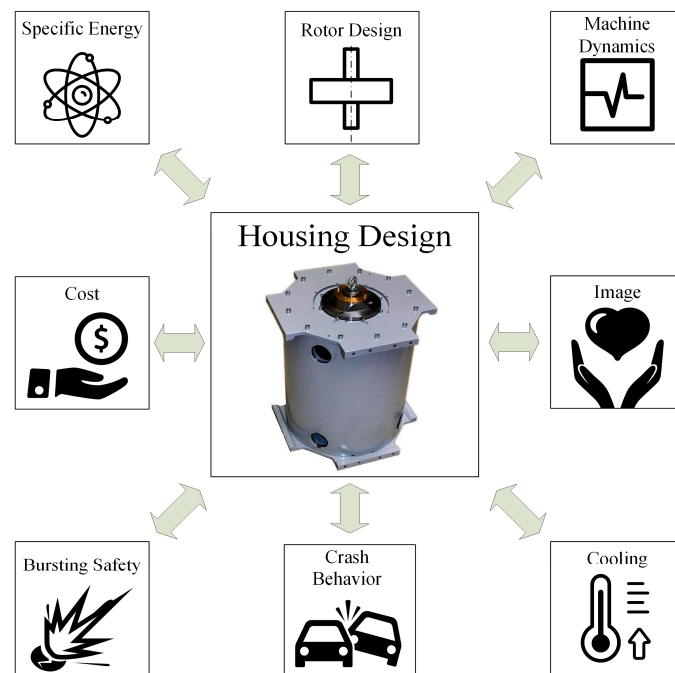


Figure 4. Eight most relevant aspects of FESS housing / containment design.

### 3. State of the Art of Burst Containments

There are three main analytic design guidelines for burst containments (specifically for FESS) presented in literature: NASA [12], Lockheed Martin [13], Genta [10]. However, the approaches and results of these calculation methods differ significantly and partially require input data, which needs to be determined empirically beforehand. Consequently, empirical validation cannot be avoided.

#### 3.1. Literature Study and Qualitative Analysis

Table 1 shows an overview of burst test data, which was gathered during a comprehensive literature study. The overview of FESS burst tests found in literature and the related qualitative analysis has led to the following conclusions:

- The number of published results of burst tests of FESS is not sufficient to allow a statistically significant qualitative analysis. Furthermore, the requirements and ambient conditions for the different tests vary significantly making it impossible to derive generally valid, proper design guidelines.
- The so-called spin tests or over-speed tests (with the goal to investigate the rotor rather than the housing) were mostly carried out in over-dimensioned, bunker-like test facilities. Investigation of designated light-weight FESS containments during vehicle crash was so far only conducted in [14], whereby the rotor was crashed but did not actually burst.
- In 2015 a publicly-funded research project on the safety of FESS housings called FlySafe was launched by the UK Research Council [15]. However, the focus is set on the investigation of the failure mechanisms of high-performance fiber composite rotors [16].

**Table 1.** Over-speed tests of steel and fiber-composite flywheels.

	Organization	Year	Description	Speed	Energy	Ref.
Steel Flywheels	Lockheed Martin	1972	Steel ring with a diameter of 515 mm and a wall thickness of 75 mm; solid steel flywheel	22,820 rpm	640 Wh	[13]
	Lockheed Martin	1972	Steel ring with 12.7 mm wall thickness and rotating liner made of GRP (178 mm thick)	16,750 rpm	340 Wh	[13]
	ETH Zürich	1996	Steel tube in concrete pit; solid steel rotor	-	-	[17]
	EMT, TU Graz	2008	Rectangular steel housing with 10 mm wall thickness and wooden lining; ceramic flywheel	8000 rpm	2,5 Wh	[11]
	Schenck Rotec/TU Graz	2014	Laminated steel rotor and steel housing consisting of 2 concentric rings with 8 mm wall thickness	45,000 rpm	280 Wh	[11]
Fiber-Composite Flywheels	Lockheed Martin	1972	Steel ring with a diameter of 515 mm a wall thickness of 75 mm	25,000 rpm	-	[18]
	Oak Ridge National Laboratory	1980	Flywheel made of fiber composite in steel housing	-	-	[19]
	ETH Zürich	1996	Wound rotor made of glass fiber rovings and epoxy matrix	-	-	[17]
	CEM, University of Texas	2002	Carbon fiber flywheel in burst containment made of aramid fibers	35,200 rpm	280 Wh	[20]
	Ricardo UK Ltd.	2016	Woven rotor made of aramid fibres for reproducible burst tests	90,000 rpm	-	[21]

Some related research was conducted in the field of turbo machinery. The findings of Hagg and Sankey [22] from the 1970s, for instance, are still relevant today in burst containment design and constantly being modified and expanded [23,24]. NASA and the U.S. Department of Transportation have also been active in the field of (aircraft) turbine containment safety design [25,26]. More recent studies dealing with turbine disc failure were published by the Zhejiang University in China [27]. Some notable FESS-specific investigations regarding containment structures were conducted by the Center for Electromechanics at University of Austin, Texas and are described for example in [20,28,29].

### 3.2. Commercially Available Test Rigs

Some companies offer industrialized spin rigs / spin pits for sale, or they offer spin services for rent. Table 2 gives an overview of some well-established companies in this field.

Apart from the companies listed in Table 2, some turbo machinery manufacturers (i.e., MAN Turbo, Rolls-Royce, MTU, etc.) and several research institutions, such as Ohio State University [30], Naval Postgraduate School [31] or NASA [32] own spin pits, which they use for their own internal

R&D activities. However, despite the seemingly large offer of test sites and equipment, the available facilities do not serve the purpose as a strategic development tool for the following reasons:

1. **Availability:** Time slots for spin tests need to be booked in advance. Availability highly depends on order situation of spin testing company.
2. **Cost:** Depending on rotor size, and desired data, a single spin test costs in the range of 1000~5000 € (Price depends on rotors size, material, burst speed and required preconditioning (balancing, heating etc.) and may well exceed 5000 € in some cases. Information is based on personal experience with European companies offering spin tests.). The purchase price of the Schenck ROTEC “Centrio 100” spin pit, for instance, is 550,000 €.
3. **Flexibility:** In order to gain deep scientific insight in the complex rotor-housing system a highly customizable test rig design regarding measurement equipment and vacuum feedthrough hardware is required.
4. **Balancing Quality:** Most commercially available spin pits require extremely accurate balancing of test rotors and do not allow burst testing of cheap rotors with low balancing quality.

**Table 2.** Commercially available spin rigs and spin testing services.

Company/Model	Offers	Specifications	Ref.
Schuster-Engineering GmbH	Customized spin pits for purchase	Specifications depend on customer requirements. Spin pits for vehicle alternators have been realized.	[33]
Schenck ROTEC GmbH/ “Centrio 100”	Spinning service and spin pits for purchase	Max. rotor diameter/length: 900/900 mm Max. rotor weight: 400 kg <sup>a</sup> Spin-testing speed: 250,000 rpm <sup>a</sup>	[34]
Schenck ROTEC GmbH/ “BI 1–7”	Spin pits for purchase	Max. rotor diameter: 200–2700 mm Max. rotor weight: 10–6300 kg <sup>a</sup> Spin-testing speed: 3000–250,000 rpm <sup>a</sup>	[34]
Test Devices Inc.	Spin pits for purchase	(No specifications available)	[35]
BSI-Barbour Stockwell Incorporated Inc.	Spinning service	Max. rotor diameter/length: 2000/1500 mm Max. rotor weight: 2.7–1800 kg Spin-testing speed: 18,000–200,000 rpm	[36]
Aerovent	Spinning service (fan wheel over-speed tests)	Max. rotor diameter: 1397/2997 mm	[37]
Oceanfront Engineers	Spinning service (compressor wheel tests)	(No specifications available)	[38]
Lingling Balancing Machinery Co Ltd./“OTS 10-1500”	Spin pits for purchase	Max. rotor diameter: 300–1500 mm Max. rotor weight: 10–1500 kg <sup>a</sup> Spin-testing speed: 9000–65,000 rpm	[39]
Piller TSC Blower Corp.	Spinning service (over-speed tests)	Max. rotor diameter/length: 1066/889 mm Max. rotor weight: 454 kg Spin-testing speed: 60,000 rpm	[40]
Element Materials Technology GmbH	Spinning service (low-cycle fatigue & burst testing)	Max. rotor diameter/length: 1600/1000 mm Max. rotor weight: 2500 kg Spin-testing speed: 65000 rpm	[41]

<sup>a</sup> Max. rotor weight and speed depends on selected gear drive. At 250,000 rpm, the max. rotor weight decreases to 10 kg.

As a consequence, in FESS rotor development spin services are usually only used for a single design validation and not as a strategic development tool during the entire design process. On the

other hand, a statistically significant number of tests would be ideal to validate numerical models and fully exploit the energy storage potential of the rotor material. This is why a low-cost test rig for spin testing was designed at the Energy Aware Systems Group at the Institute of Electrical Measurement and Measurement Signal Processing (Graz University of Technology).

#### 4. Low-Cost Spin Pit Design

In this section the initial test rig design is described, including the main issues that occurred during commissioning, followed by the measures taken to solve them. The design process of the test rig was dominated by a consequent low-cost approach, which was based on the following requirements:

- Using economic off-the-shelf components
- Simple manufacturing of custom-made parts (machinable with standard tooling)
- Minimizing test specimen setup-time and assembly/disassembly effort
- Smart concept using separable joints and few (as well as cheap) consumable parts
- High flexibility regarding burst containment dimensions through modular design
- Guaranteed safety achieved by the use of massive outer test rig housing
- Accurate determination of energy content at rotor burst

##### 4.1. Rotor Dynamics and Design Considerations

When designing high-speed rotating machines, such as the test rig described in this paper, rotor dynamics is of high importance. Section 4.1.1 describes some lessons learned during commissioning of the initial design, which is shown in Figure 5.

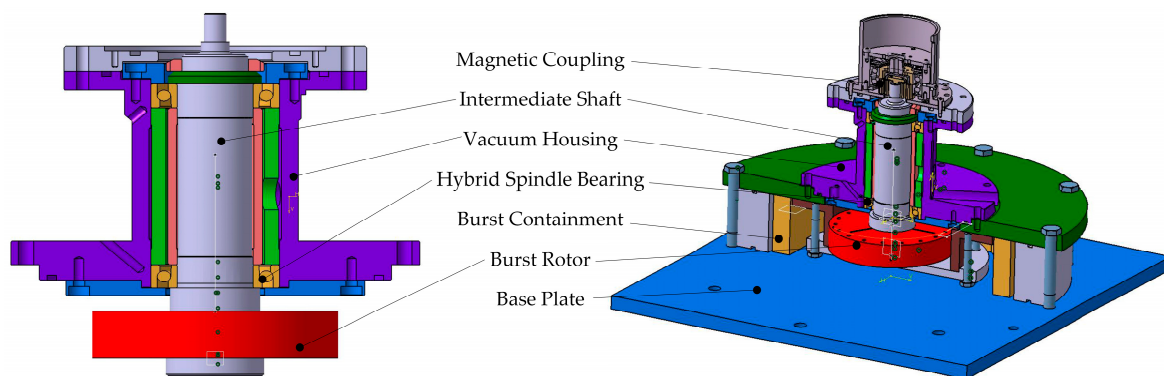


**Figure 5.** Initial test rig design intended to allow under-critical rotor operation.

##### 4.1.1. Initial Test Rig Design

The initial test rig was designed to be operated below the first eigenfrequency (i.e., undercritical rotor operation), the desired burst speed of the test flywheel (described in Section 4.2.2) was calculated by finite element analysis (FEA) to be around 30,000 rpm. In order to realize sub-critical operation, the system required high overall stiffness. To reach the required system stiffness and speed capability, axially pre-stressed hybrid spindle bearings with an inner diameter of 40 mm mounted on a massive intermediate shaft were used. Air drag losses were reduced through operation of the rotor and intermediate shaft under low pressure environment (5 mbar vacuum). A bell-shaped magnetic coupling was used to transmit the torque from the motor, which was located outside at ambient pressure, to the intermediate shaft inside the vacuum chamber (see Figure 5) The burst rotor of the initial design is presented in Section 4.1.2.

##### 4.1.2. First Commissioning

During first commissioning of the test rig two major issues occurred:



## 1. Rotor dynamics issue

The real overall system stiffness was lower than calculated by FEA, because the following properties showed strong deviation between the CAD model and the actual test rig:

- Contact stiffness of the system setup (including bearing seats) was lower than calculated due to surface roughness and tolerancing.
- The real bearing stiffness is speed-dependent, which was neglected in the FEA analysis.
- Frame rigidity and foundation are in reality not infinitely stiff as assumed in the model.

As a result, the first eigenfrequency was found to be below burst speed. With the selected drive (electric spindle motor—see Section 4.2.1) it was not possible to run through the resonance, resulting in high deflection amplitudes of the intermediate shaft, which caused contact between the separating bell of the magnetic coupling and the rotor leading to a destruction of the magnetic coupling. Figure 6a gives an impression, of the coupling after system failure.

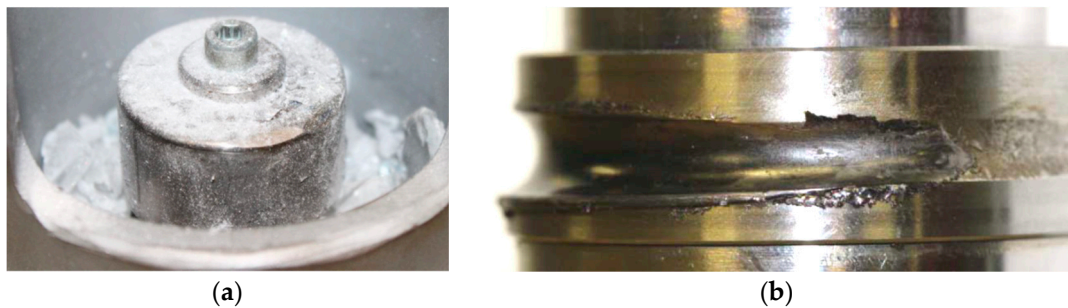


**Figure 6.** (a) Broken magnetic coupling in glass debris of containment shroud; (b) damaged bearing race.

## 2. Rotor Design Issue

A special burst rotor design, which allows for an accurate setting of burst speed was intended to achieve reproducible burst conditions. To overcome uncertain material properties (e.g., varying tensile strength resulting from inhomogeneity and varying alloy composition) the rotor was notched on the inner diameter, where the highest stresses appear. Figure 7 shows an image of the rotor.

At high speeds the centripetal forces caused the interference fit between the shaft and the hub of the rotor to detach because of plastic deformation. Main reason was the notched rotor design in combination with a highly ductile rotor material (mild steel). Due to the material's ductility, no sudden fracture was achieved as desired, but the rotor plasticated locally, was released from the shaft and could not be accelerated further to burst speed.

In the second attempt, the rotor did not detach, but the emerging rotor imbalance increased bearing loads to impermissible levels causing the SiNi rolling elements of the spindle bearing to fracture. A picture of the inner bearing race after bearing failure is shown in Figure 6b. Figure 7 shows an image of the initial rotor design including rotor properties.

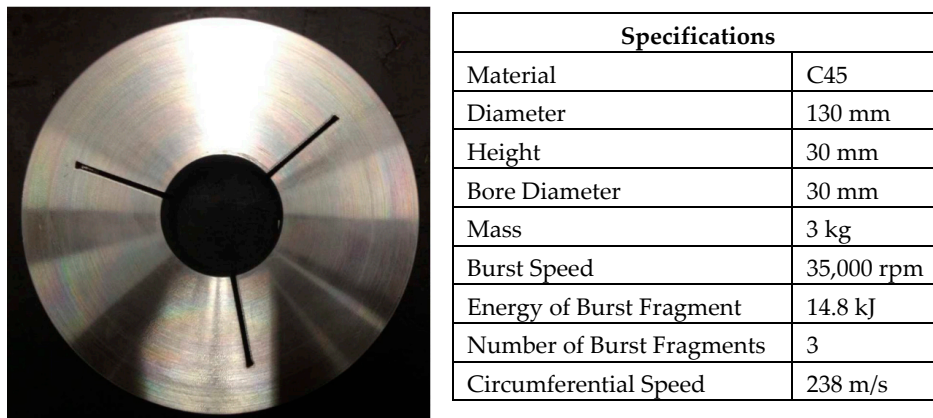


**Figure 7.** Initial burst rotor design and relevant properties.

#### 4.1.3. Design Iteration

In order to overcome the issues described in Section 4.1.2 the design was improved regarding the following aspects:

##### (a) Solving the rotor dynamics issue

Instead of sub-critical operation the concept was changed to super-critical operation. This was achieved by drastically reducing the overall system stiffness by using a thin, flexible quill shaft connecting the intermediate shaft with the burst rotor (indicated in yellow in Figure 8). As a result, the first eigenfrequency shifted to very low speeds (few hundred rpm depending on rotor mass) and low oscillation energy levels, eliminating problems during resonance run-through. At super-critical operation the rotors self-centering characteristics enabled stable operation while accelerating the rotor to burst speed.

Since high system stiffness was not required anymore, the intermediate shaft could be down-sized. Another positive aspect was the mechanical decoupling of rotor and intermediate shaft loads. As a result, smaller and much cheaper angular contact ball bearings could be used instead of hybrid spindle bearings to reach rotational speeds sufficiently high for rotor burst (In this case, rotor burst speeds of 20,000 to 40,000 rpm are desired.). Furthermore, the total moment of inertia of all rotating test rig parts decreased, allowing the system to reach burst speed faster.

Using a disc-shaped instead of bell-shaped magnetic coupling reduced cantilevered rotor mass, desensitizing the drive unit against deflections caused by rotor dynamics and increasing system robustness.

##### (b) Solving the rotor design issue

The burst rotor (i.e., test flywheel) was redesigned to solve the issues, which arose during first commissioning. The new design, which is described in more depth in Section 4.3, is a single mill-turned part with notches for pre-defined fragment geometry. The new test flywheel not only allows more accurate adjustment of the burst speed, but also solved the issues related to the interference fit by introducing a clamp set with small router diameter (14 mm), hence eliminating imbalance forces caused by play between shaft and rotor.

##### (c) Additional considerations

Because of the new, flexible quill shaft with little damping, higher deflections were expected during resonance run-through depending on rotor balancing quality. To limit rotor oscillation amplitude, a trunnion was added at the bottom of the burst rotor, which runs in a safety gliding bearing.

The flexible shaft was attached to the intermediate shaft using a standard collet (concentricity: 2  $\mu\text{m}$ ) to ensure assembly accuracy and pursue consequent low-cost design.

A detachable coupling (clamp set “CLAMPEX KTR131” [42]) was used to connect the burst rotor to the flexible shaft.

#### 4.2. Final Design

The final test rig design, as shown in Figure 8, can be divided into four main modules, which are described below. The periphery (sensors, data acquisition systems, signal amplifier, lifting winches, etc.) is considered lab equipment and not part of this analysis. However, information can be provided on request by contacting the authors.

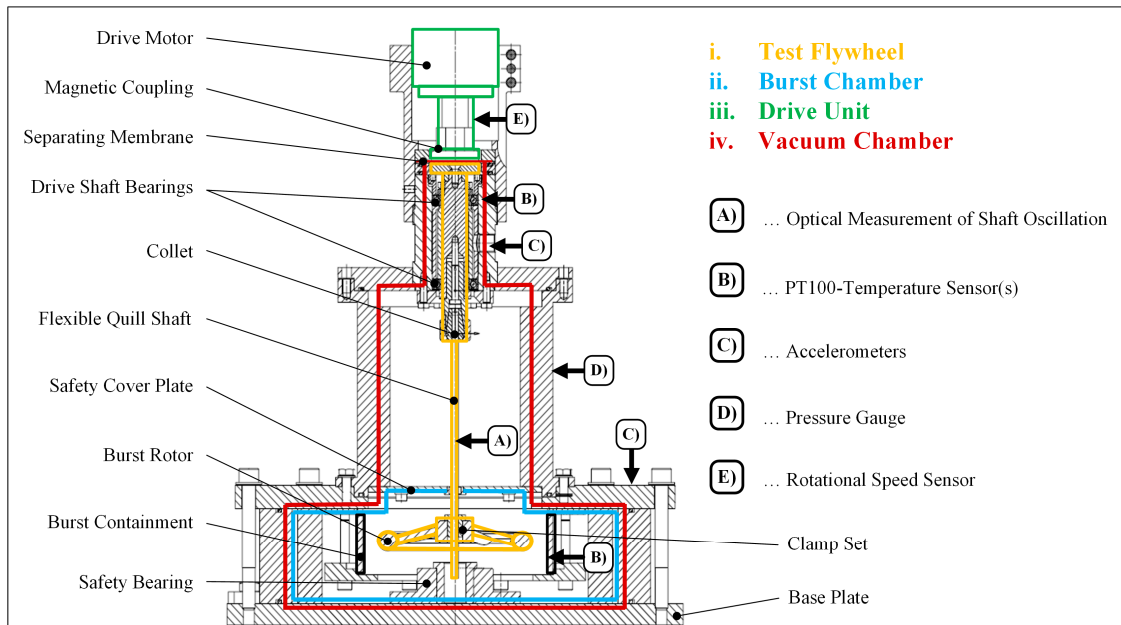


**Figure 8.** Schematics of the burst test rig (final design) including measurement technology.

##### i. Test Flywheel (orange)

The test flywheel, which will be deliberately destroyed during the burst test is fixed on a flexible, cantilevered quill shaft via a clamp set. On the one hand, resonance frequency and the influence of imbalance forces are mitigated, on the other hand peak forces during rotor burst can hardly be transmitted to the spindle bearings and drive unit. The flexible, 6 mm thick quill shaft is fed through a safety cover plate, to avoid the entering of rotor debris towards the bearings system.

##### ii. Burst Chamber (blue)

The burst chamber accommodates the burst containment under investigation. In the current configuration, these test specimens are cylindrical metal parts with a fitted key to avoid rotation during fragment impact. The exact geometry of the burst containment is shown in Section 5.2.

The outer walls of the test rig’s burst chamber are made of 25 mm solid steel. The safety bearing (a sliding bearing made from polytetrafluoroethylene—PTFE), which limits excessive oscillation and plastic deformation of the quill shaft during resonance run-through, is fixed in the center of the base plate.

##### iii. Drive Unit (green)

The electric spindle motor (asynchronous machine and variable frequency drive by the company Mechatron) provides a maximum power of 2.2 kW and 42,000 rpm. This motor was already available at the authors’ Energy Aware Systems lab. The electric motor listed in Table 3 represents a lower cost

alternative with similar performance. The torque is transmitted to the shaft via disc magnetic coupling, which allows hermetical sealing of the burst chamber from the environment.

#### iv. Vacuum Chamber (red)

Evacuating the burst chamber is mostly necessary for two reasons:

- Aerodynamic drag of the test flywheel would require much higher torque capabilities of the drive system if operated at ambient pressure.
- Viscous damping and gas friction may influence the results of the burst tests.

The pressure level can be lowered to around 0.5 mbar by using a simple two-stage rotary vane pump.

A photograph of the final setup including data acquisition and periphery is shown in Figure 9.

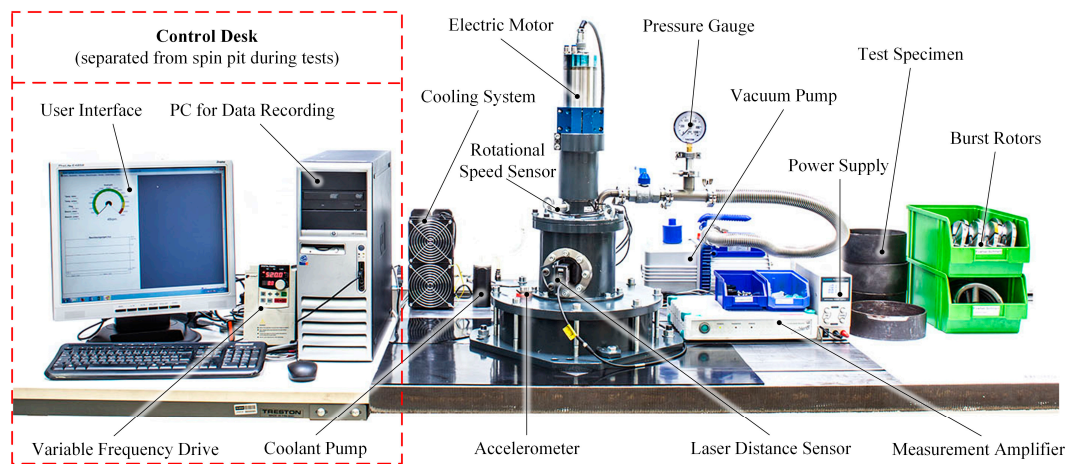


**Figure 9.** Low-cost spin pit and major components including periphery. Please note that the control desk (left) is moved away from the test rig when burst tests are conducted.

#### 4.2.1. Off-the Shelf Parts and Components

In order to keep costs low, the number of custom parts was reduced to a minimum. This consideration is applied to the test rig design as well as to the test specimen. Table 3 shows the off-the-shelf components used in the final test rig (excl. test rotor, which is described in Section 4.3).

**Table 3.** Off-the-shelf components used in drive unit, mechanical connections, and cooling system.

Component	Name or Brand	Price	Specifications	Ref. <sup>a</sup>
Motor + variable frequency drive	Spindle: SDK80-48Z-1.5 VFD: FC300-2.2T2	900 €	P = 1.5 kW $n_{\max} = 48,000$ rpm	-
Clamp set	KTR 131	25 €	Self-centering $\varnothing 6$ mm	[42]
Shaft	6 mm shaft, CF53, material code: 1.1213	5 €	300 mm $\times$ $\varnothing 6$ mm $\times$ 6 h	-
Magnetic coupling	MTD 0.3 Mobac	130 €	$n_{\max} = 26,000$ rpm $M_t = 1.12$ Nm @ 3 mm gap	[43]
Rolling bearing (2 required)	71905 CDGA/P4A	100 €	$n_{\max} = 44000$ rpm	[44]
Radiator	240 mm computer water cooling radiator	16 €	276 $\times$ 120 $\times$ 32 mm	-
Adapter	2 $\times$ external thread fitting adapter	3 €	G 1/4 Thread	-
Coolant hose	2M transparent soft PVC tube	9 €	9.5 $\times$ 12.7 mm tube	-
Pump + expansion tank	Coolant water pump + expansion tank	30 €	Flow rate: 500 L/h	-
Fan (2 required)	Standard 120 mm PC-Fan	12 €	120 $\times$ 120 $\times$ 38 mm, 230 V AC	-
Total cost of off-the-shelf components		1345 €		

<sup>a</sup> if no reference is given, the information was taken from ebay.com.

#### 4.2.2. Overall Test Rig Costs

Main cost driver of the off-the-shelf components is the electric motor with the required variable frequency drive. Depending on the requirements regarding maximum speed and power, different options may be considered for the test rig setup. Compared to the custom-made parts (shown in Table 4), these components have an overall cost share of about 23%.

The following statement of costs includes only tailored (custom-made) parts referred to the four sub-systems defined in Figure 8.

**Table 4.** Custom components used in the test rig.

Sub-System	Machined Parts	Cost
Test flywheel + intermediate shaft	Test flywheel, intermediate shaft, tailored collet, bearing periphery	610 €
Vacuum chamber	Housing, intermediate flange, motor mount interface, base plate	2860 €
Drive unit	Magnetic coupling membrane, motor mount	420 €
Burst chamber	Safety cover plate, containment support, and fitted key	650 €
Total cost of custom components		4540 €

Including off-the-shelf components, the costs for the whole test rig amounts to less than 5900 € excluding assembly, test specimen (i.e., burst rotors, flywheels), and operating costs.

#### 4.3. Test Specimen and Operating Costs

Initially, a complex mill-turned part (Figure 10 (left)) was used as test flywheel. The design allowed precise adjustment of burst speed due to a weakening groove and pre-defined fragment geometry by milling a radial notch. In order to reduce operating costs and allow for a high number of tests, a low-cost alternative was found by using off-the-shelf hand wheels made from grey cast iron (Figure 10 (right)), which served the purpose surprisingly well. When operating a rotor on a flexible, cantilevered shaft, close attention must be paid to the ratio of the moments of inertia ( $J_1$ —around the main axes of rotation and  $J_2$ —perpendicular to it). According to the authors’ experience a ratio of  $J_1/J_2$  between 0.8 and 1.2 must be avoided, or else instabilities might occur. The properties of the test flywheels are compared in Table 5.

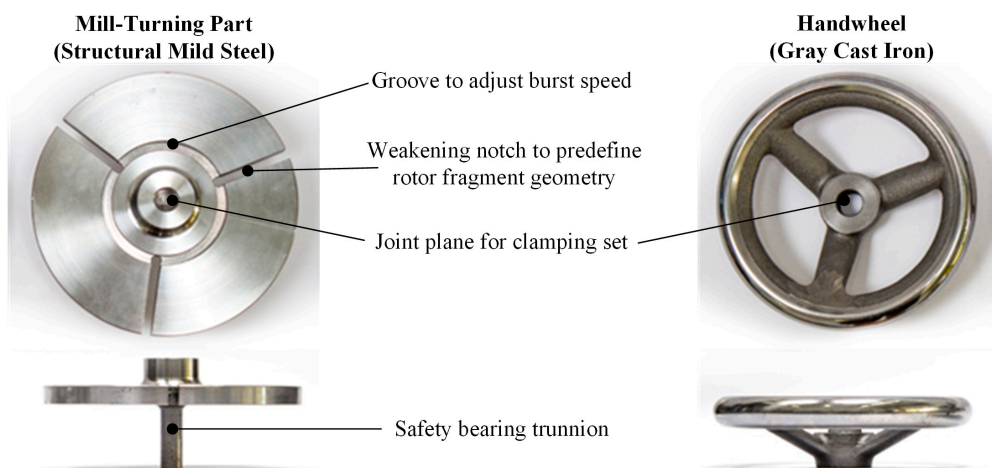


**Figure 10.** Burst rotors, (left) mill-turned part; (right) low-cost alternative (cast iron hand wheel).



Determination of inherent kinetic energy during burst is possible in both cases (post mortem analysis) as described in more detail in Section 5.

**Table 5.** Comparison of properties—Custom-made mill-turned rotor vs. off-the-shelf cast iron hand wheel.

Component	Custom-Made Rotor	Hand Wheel
Material	C45E	Gray Cast Iron
Diameter	139 mm	140 mm
Height (excl. hub and trunnion)	10 mm	17 mm
Total mass	1180 g	1000 g
Burst speed <sup>a</sup>	~29,000 rpm	25,000~31,500 rpm
Energy of single burst fragment	~3950 J	900~1500 J
Number of fragments	3	6~9
Circumferential speed	210 m/s @ 29,000 rpm	175 m/s @ 27,000 rpm
Cost per unit	120 €	14 €

<sup>a</sup> Burst speed can be set by weakening groove or notch. Casted hand wheel has greater variation due to shrinkage cavities.

### Replacement Parts

After every burst the test flywheel, the mechanical coupling, and the flexible quill shaft need to be replaced (in addition to the burst containment under investigation). To reduce running costs, the KTR131 coupling (which connects the flexible quill shaft to the test flywheel and is shown in shown in Figure 11a) was replaced by a new custom clamping design shown in Figure 11b. The robust design ensures longevity and reduces operating costs to 19 € per burst, corresponding to a reduction of 57%.

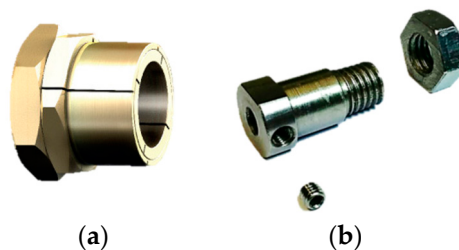


**Figure 11.** (a) KTR Clampex 131, (b) custom made alternative.

### 5. Test Procedure and Evaluation Methods

The goal of the empirical investigation lies in the determination of an analytic relation between the kinetic energy of the rotor (or rotor fragments) and the energy absorption ability of the burst containment/housing while retaining structural integrity, as well as validation of numerical models in the long run. Ultimately, the developed methods will allow the design of safe, yet light-weight housings for high-speed rotating machines.

Using the test rig and the test flywheels described in Sections 4.2 and 4.3 respectively, the actual burst test (i.e., accelerating the specimen to rotational speeds, at which the centripetal stresses exceed the material's tensile strength) takes around 15 s. This value may vary depending on balancing quality and moment of inertia of the test flywheel (and related resonances) and refers to the drive unit specifications presented in Section 4.2. During the acceleration process, rotational speed, radial acceleration of bearing seats and oscillation of the quill shaft are monitored and recorded (for instrumentation, see Figure 8). Data processing and analysis, on the other hand, is far more time consuming and consists of the four main steps described below.



### 5.1. Documentation and Reconstruction

The process starts with an in-situ photo documentation, after which the rotor fragments are re-assembled and matched with the impact marks of the containment. This procedure is used in the case of the grey cast iron hand wheels and does not necessarily apply to all other possible test flywheels. Thorough investigation of skid marks on rotor and housing, and in some cases color marks, allow identification of rotor crack initiation. Applying this technique, it can be determined whether the rotor fragments were formed due to centripetal forces or broke again during impact. The structure of the process and some examples are shown in Figure 12.

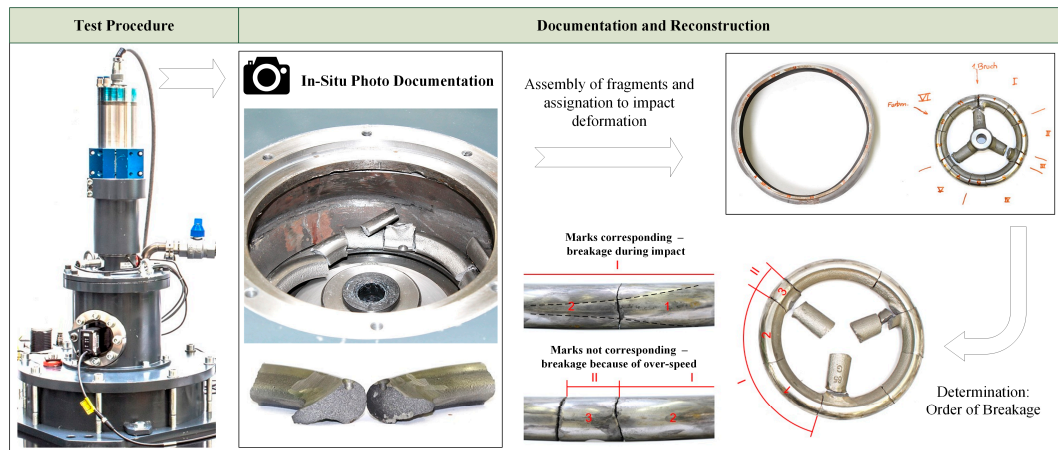


Figure 12. Step 1—Documentation and reconstruction.

### 5.2. Survey of the Burst Containment

The plastic deformation work, which is introduced in the burst containment is a measure for its ability to absorb energy. If the containment was punctured or broken through, there is no possibility to deduce the energy which was absorbed, since part of the fragment’s kinetic energy was absorbed during impact in the spin pit. In all other cases, the plastic deformation work is determined by comparison of the containment geometry before and after impact, as shown in Figure 13. Originally this was achieved by measuring the circumference of the containments at different heights and interpolating the contour by a polynomial of fourth order. Later, 3D-scanning of the burst containment before and after the test was introduced to allow numerical determination of the deformation rate (compare Figure 14.)

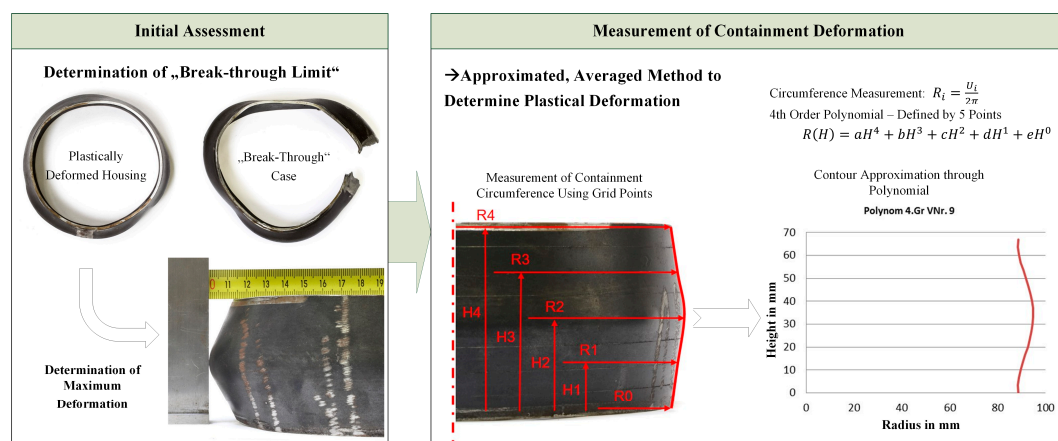


Figure 13. Step 2—Survey of containment deformation.

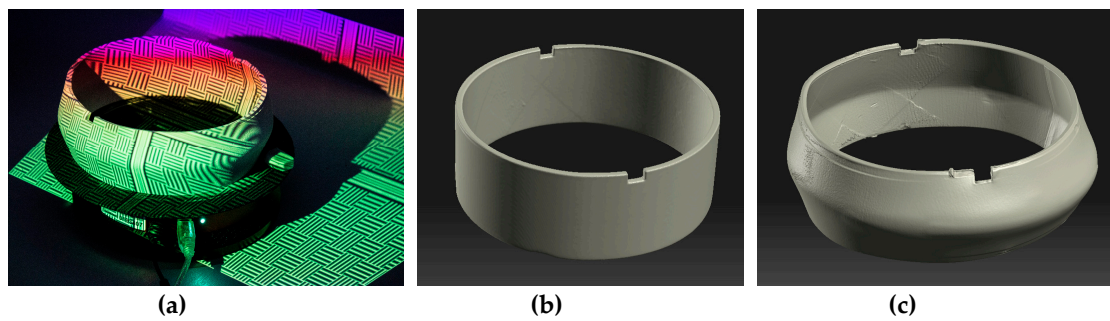


Figure 14. 3D-scanning of burst containments (a) including results before (b) and after (c) burst.

### 5.3. Mathematical Evaluation

The goal, as mentioned previously, is to find out and establish a relation between the kinetic energy of the rotor fragments and the energy absorption ability of the containment. In this context, it is essential to determine the shares of rotational and translational energy of each fragment as shown in Figure 15, since the translational share is predominantly responsible for safety containment deformation (in radial direction). The fewer parts, the higher the rotational share is.

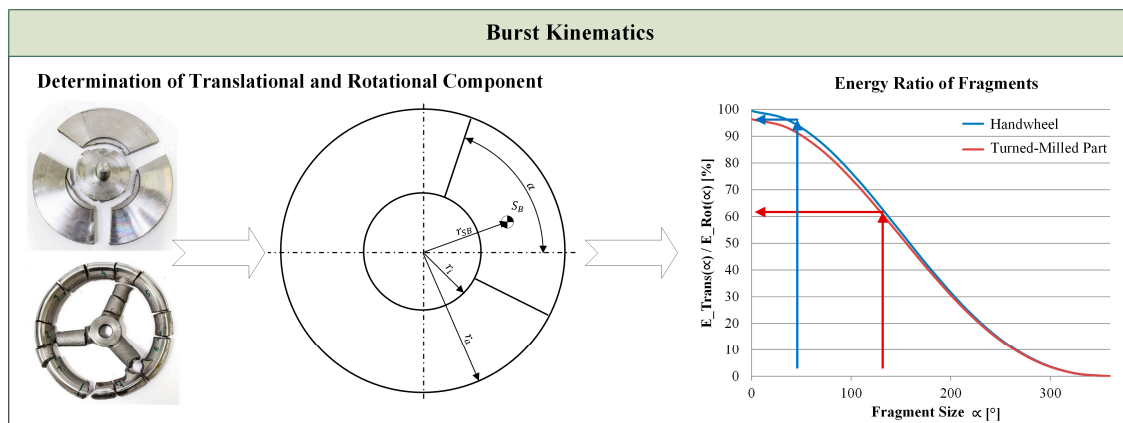


Figure 15. Step 3a—Determination of rotor fragment geometry and shares of energy.

Surface enlargement through plastic deformation can be determined in 2 ways:

- (a) It can be approximated analytically by measuring the circumference of the housing at several heights and summing up the surface area of several conical shells.
- (b) It can be determined numerically by comparing the 3D-scanned (as shown in Figure 14).
- (c) surface with the initial, undeformed cylinder. The surface area can be determined using automated functions of commercial CAD software such as Dassault Systems CATIA, Siemens NX, or Autodesk Inventor.

The strain  $\epsilon$  of the containment is identified by comparison of the initial cylindrical surface area with the deformed surface area after burst. With a stress–strain diagram of the containment material at hand, the plastic deformation work can then be calculated as the area under the “ $\sigma\epsilon$ -curve” as shown in Figure 16 on the right.

However, it must be mentioned that these stress–strain diagrams are usually determined using a quasi-static tensile test and dynamic effects of the ballistic impact, which usually only last a few milliseconds, are neglected (A test flywheel with a diameter of 140 mm has a rim speed of approx. 220 m/s at 30,000 rpm. Rotor fragments traveling at this speed are decelerated to zero within only a few millimeters or centimeters at the most.). The strain-rate-dependent inelastic behavior of materials is called viscoplasticity [45]. Neglecting effects such as strain hardening [46] may result in

inaccuracies in the overall energy balance of the burst housing. This error can be approximated using numerical simulations based on a Johnson–Cook material model [47], but actual measured material data at these high deformation speeds is not available for any desired material. Since the scope of this paper is to address spin pit design and operation and not FEM simulations, more detailed information on data analysis and actual burst containment design will be published separately or can be acquired by contacting the authors. However, the basic principle of the evaluation of plastic deformation work is shown in Figure 16.

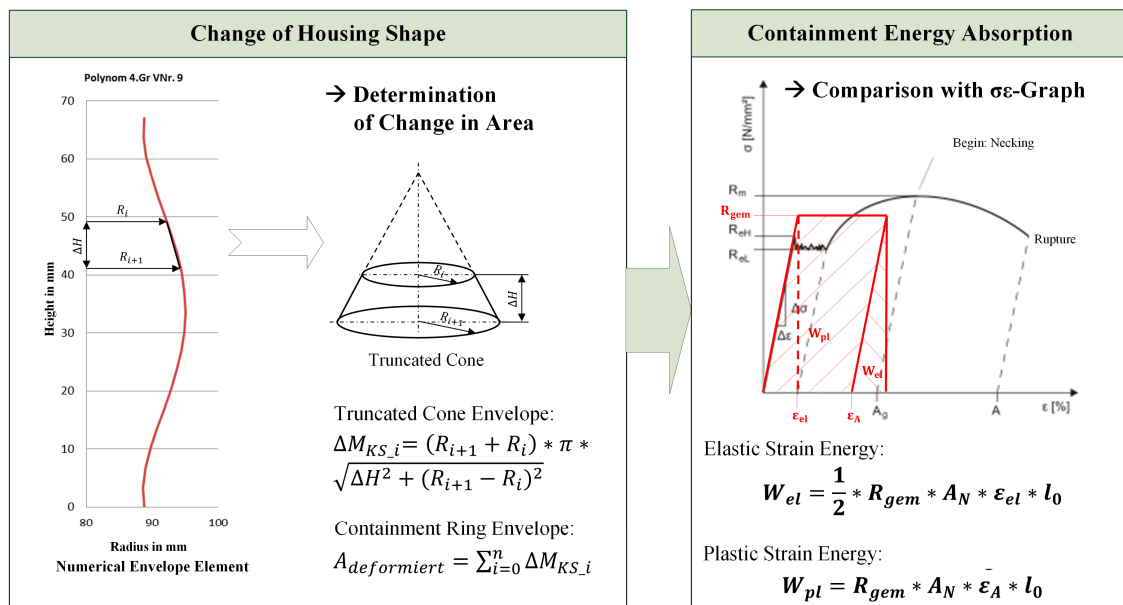
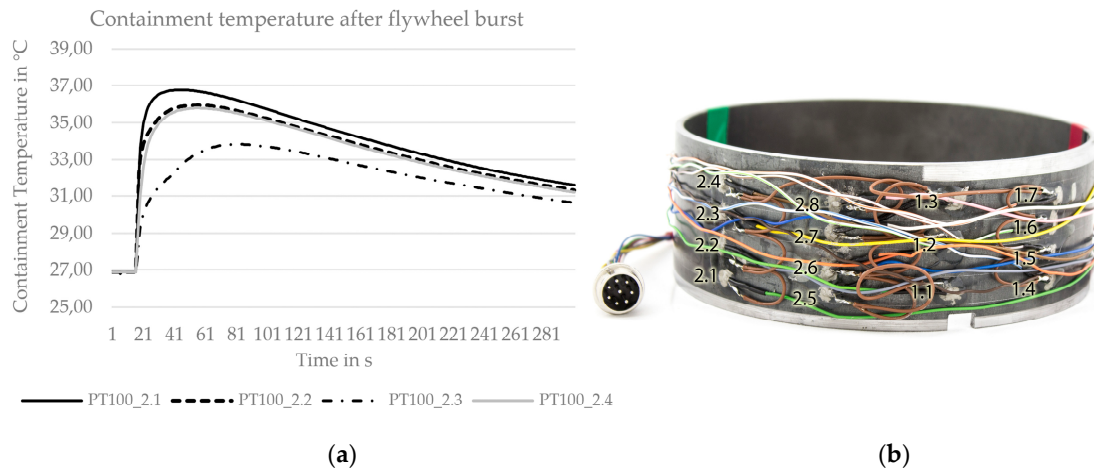


Figure 16. Step 3b—Determination of plastic deformation work of the burst containment.

#### 5.4. Energy Balance

After the deformation work has been determined, other terms of the energy balance such as heat dissipated, as well as generation of surface area due to crack propagation in the rotor fragments during impact are considered. The latter can be determined via a notch-impact test of samples made from the same material as the rotor. Temperature entry in the housing on the other hand was measured directly by applying temperature sensors to the housing as shown in Figure 17a. An example for the temperature increase during impact is shown in Figure 17b.



**Figure 17.** (a) Temperature increase after flywheel burst, showing the measurements of sensors 2.1 to 2.4 referring to the pictured containment; (b) Burst containment equipped with 15 temperature sensors (PT100).

Figure 17 (left) shows that a maximum temperature increase of around 10 °C is reached immediately after impact, then the temperatures slowly drop again due to heat conduction. Since the actual spin pit is evacuated, there is no convective cooling of the burst containment and radiation can be neglected at these low temperatures. Hence, the energy transformed into heat  $E_t$  can be calculated via

$$E_t = m_h * c_p * \Delta t \tag{3}$$

With  $m_h$  being the mass of the burst containment,  $c_p$  the specific heat capacity and  $\Delta t$  the maximum temperature difference.

## 6. Summary of Results

The test rig described in Section 4 allows to conduct rotor burst tests and containment investigation at such low cost, that statistically significant results can be produced. This low-cost spin pit hence represents a strategic development tool for safety housings of high-speed rotating machines.

Figure 18 shows a burst containment after testing and the related calculated energy balance, indicating the different shares of energy entry. Please note that the plastic deformation work is mainly comprised of thermal energy and a small share (around 10%) of elastic tensioning. The relatively large unknown share may be explained by effects such as:

- Containment rotation (slipping) like a rotational liner.
- Friction between fragments and base-plate or lid of burst chamber.
- Elastic tensioning/deformation, which makes the fragments bounce around in the spin pit.
- Elastic deformation of other test rig parts.

Approaches to quantify these phenomena are currently under investigation.

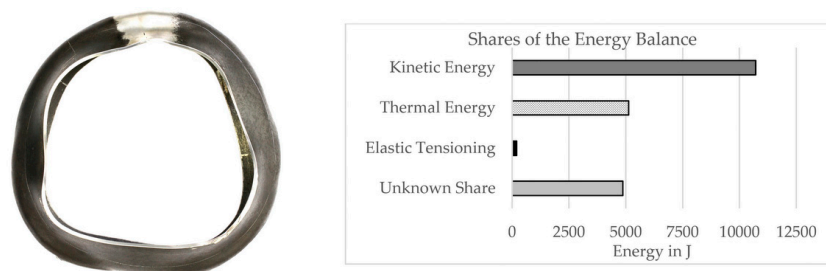


**Figure 18.** Burst containment and corresponding energy balance showing the shares, in which the kinetic energy of the rotor is transformed into.

So far, dozens of burst tests have been completed with the current setup and no significant damage to the test rig has occurred. Different containment thicknesses and materials, such as mild steel, stainless steel, and aluminum have been successfully tested.

## 7. Discussion

Even though high-speed rotating machines play an increasingly important role in all fields of technology, ranging from electric drives to turbines, data on rotor burst and respective containment performance can hardly be found in literature. According to the authors' knowledge, this paper is the first to describe the design process and operation of a low-cost test rig for burst containment investigation.

The consequent low-cost design and the detailed description of the test rig allows other researchers to copy this setup for system costs below 6000 €, which is extremely low compared to the costs of industrial burst tests that may amount up to several thousand Euro (compare Section 3.2). Granting access to a low-cost spin pit as strategic development tool will boost research and insight in the field of failure mechanics, rotor dynamics, and containment design, as well as the safety of rotating machinery in general and is hence a valuable contribution to the scientific community.

Future research of the authors will include:

- Investigation of more sophisticated/complex containment structures (rotating liners, composite material, energy absorbing structures such as aluminum foam, etc.)
- Determination of an analytic approximation formula describing the relation between kinetic flywheel energy and energy absorbing properties of the containment
- Validation of numerical models (e.g., in ABAQUS)

## 8. Conclusions

The development process of a low-cost test rig for the investigation of burst containments for high-speed rotation machines was presented in detail, including its design process and operation. Design considerations such as rotor dynamics and operating costs, as well as test specimen design were also presented in Section 4 to help other researchers avoid mistakes and benefit from lessons learned during this project. A thorough investigation of the state of the art (compare Sections 3.1 and 3.2) has shown that there is no information on similar low-cost spin pits available. However, the demand for such test rigs (and/or services) is high as rotational speeds of machines (e.g., turbines, electric motors, and flywheel energy storage systems) are ever increasing for reasons of light-weight engineering and improved power/energy densities.

**Author Contributions:** Conceptualization, Methodology and Writing-Original Draft Preparation, A.B.; Formal Analysis and Validation, P.H.; Data Curation and Investigation, C.B.; Software and Validation, T.Z.; Resources and Funding Acquisition, H.W.

**Funding:** This research was funded in part by the Austrian Research Promotion Agency (FFG) within the Electric Mobility Flagship Projects, 9th call, grant number 865447.



**Acknowledgments:** The authors would like to thank Michael Bader, Stefan Burgholzer, Thomas Atzlinger, Martin Jungreithmair, Thomas Czerwinka, and Roland Rieger for their support during the early design stages of the test rig and their advice regarding improvements. The authors would also like to thank all members of the Energy Aware Systems Group led by Hannes Wegleiter for the valuable discussions regarding measurement equipment and data acquisition.

**Conflicts of Interest:** The authors declare no conflict of interest.

## References

- Buchroithner, A.; Haan, A.; Preßmair, R.; Bader, M.; Schweighofer, B.; Wegleiter, H.; Edtmayer, H. Decentralized Low-Cost Flywheel Energy Storage for Photovoltaic Systems. In Proceedings of the International Conference on Sustainable Energy Engineering and Application (ICSEEA 2016), Jakarta, Indonesia, 3–5 October 2016.
- Arani, A.A.K.; Karami, H.; Gharehpetian, G.B.; Hejazi, M.S.A. Review of Flywheel Energy Storage Systems structures and applications in power systems and microgrids. *Renew. Sustain. Energy Rev.* **2017**, *69*, 9–18. [[CrossRef](#)]
- Amiryar, M.E.; Pullen, K.R. A Review of Flywheel Energy Storage System Technologies and Their Applications. *Appl. Sci.* **2017**, *7*, 286. [[CrossRef](#)]
- Buchroithner, A.; Jürgens, G. Flywheel Energy Storage—An Opportunity for the Automotive Industry and Beyond. In Proceedings of the 38th International Vienna Motor Symposium, Vienna, Austria, 27–28 April 2017; Volume 2, pp. 432–451.
- Buchroithner, A.; Wegleiter, H.; Schweighofer, B. Flywheel Energy Storage Systems Compared to Competing Technologies for Grid Load Mitigation in EV Fast-Charging Applications. In Proceedings of the 27th International Symposium on Industrial Electronics (ISIE), Cairns, Australia, 12–15 June 2018.
- Bender, D. *Recommended Practices for the Safe Design and Operation of Flywheels*; Sandia Report; National Nuclear Security Administration: Washington, DA, USA, 2015.
- Wikinvest.com. Safety Failures by the Company’s Flywheel Products or Those of Its Competitors Could Reduce Market Demand or Acceptance for Flywheel Services or Products in General. Available online: [http://www.wikinvest.com/stock/Beacon\\_Power\\_%28BCON%29/Safety\\_Failures\\_Flywheel\\_Products\\_Those\\_Competitors\\_Reduce\\_Market](http://www.wikinvest.com/stock/Beacon_Power_%28BCON%29/Safety_Failures_Flywheel_Products_Those_Competitors_Reduce_Market) (accessed on 14 May 2016).
- Flint, D. *A Mishap at the Beacon Power Frequency Flywheel Plant*; The Eastwick Press: Petersburg, NY, USA, 2011.
- Mento, T.; Ruth, B. Injuries Reported in Explosion at Poway Business. *KPBS Public Broadcasting*, 11 June 2015.
- Genta, G. *Kinetic Energy Storage: Theory and Practice of Advanced Flywheel Systems*; Butterworth-Heinemann: London, UK, 1985.
- Buchroithner, A. Improved Efficiency of Flywheel Energy Storage in Vehicles through Interdisciplinary and Multi-Dimensional Optimization of Their Sub- and Supersystem. Ph.D. Theses, Graz University of Technology, Graz, Austria, 2017; p. 161.
- Colozza, A.J. *High Energy Flywheel Containment Evaluation*; NASA: Brook Park, OH, USA, 2000.
- Gilbert, R.R.; Heuer, G.E.; Jacobsen, E.H.; Kuhns, E.B.; Lawson, L.J.; Wada, W.T. *Flywheel Drive Systems Study—Final Report*; Environmental Protection Agency: Washington, DC, USA, 1972.
- Green Car Congress. Flybrid Flywheel Hybrid System Passes First Crash Test. 2007. Available online: <http://www.greencarcongress.com/2007/10/flybrid-flywhee.html> (accessed on 19 September 2010).
- Research Councils UK/Innovate UK. FlySafe—Flywheel-Hybrid Safety Engineering. United Kingdom. Available online: <https://gtr.ukri.org/projects?ref=101306> (accessed on 20 October 2018).
- Nicolas, R. A New Flywheel Test Rig Developed by Ricardo, 6 July 2015. Available online: <http://www.car-engineer.com/a-new-flywheel-test-rig-developed-by-ricardo/> (accessed on 22 July 2016).
- von Burg, P. *High-Speed Flywheel Made of Fiber Composite (“Schnelldrehendes Schwungrad aus Faserkunststoff”)*; ETH Zürich: Zürich, Switzerland, 1996.
- Renner-Smith, S. Battery-saving flywheel gives electric car freeway zip. *Pop. Sci.* **1980**, *215*, 82–84.
- Oak Ridge National Laboratory. Oak Ridge National Laboratory Review. Oak Ridge National Laboratory’s Communications and Community Outreach. Available online: <http://web.ornl.gov/info/ornlreview/rev25-34/chapter8.shtml> (accessed on 25 August 2016).
- Pichot, M.A.; Kramer, J.M.; Thompson, R.C.; Hayes, R.J.; Beno, J.H. *The Flywheel Battery Containment Problem*; Society of Automotive Engineering: Warrendale, PA, USA; Troy, MI, USA, 1997.



21. Wheals, J.; Taylor, J.; Lanoe, W. Rail Hybrid using Flywheel. In Proceedings of the Den Danske Banekonferencen, Copenhagen, Denmark, 17 May 2016.
22. Hagg, A.C.; Sankey, G.O. The Containment of Disk Burst Fragments by Cylindrical Shells. *J. Eng. Power* **1974**, *96*, 114–123. [[CrossRef](#)]
23. Stamper, E.; Hale, S. The Use of LS-DYNA®Models to Predict Containment of Disk Burst Fragments. In Proceedings of the 10th International LS-DYNA®Users Conference, Dearborn, MI, USA, 8–10 June 2008.
24. Klimaszewski, S.; Woch, M. Modified hagg & sankey method to estimate the ballistic behaviour of lightweight metal/composite/ceramic armour and a fuselage skin of an aircraft. *J. KONES Powertrain Transp.* **2012**, *19*, 245–252.
25. Collins, T.P.; Witmer, E.A. *Application of the Collision-Imparted Velocity Method for Analyzing the Responses of Containment and Deflector Structures to Engine Rotor Fragment Impact*; Aeroelastic and Structures Research Lab.: Cambridge, MA, USA, 1973.
26. Mathis, J.A. *Design Procedures and Analysis of Turbine Rotor Fragment Hazard Containment*; U.S. Department of Transportation—Federal Aviation Administration Final Report; Office of Aviation Research: Washington, DC, USA, 1997.
27. Xuan, H.; Liu, L.; Feng, Y.; He, Q.; Li, J. Containment of high-speed rotating disk fragments. *J. Zhejiang Univ. Sci. A* **2012**, *13*, 665–673. [[CrossRef](#)]
28. Dulaney, K.A.; Beno, J.H.; Thompson, R.C. Modeling of Multiple Liner Containment Systems for High Speed Rotors. *IEEE Trans. Magn.* **1999**, *35*, 334–339. [[CrossRef](#)]
29. Strubhar, J.L.; Thompson, R.C.; Pak, T.T.; Zierer, J.J.; Beno, J.H.; Hayes, R.J. Lightweight Containment for High-Energy Rotating Machines. *IEEE Trans. Magn.* **2003**, *39*, 378–383. [[CrossRef](#)]
30. Ohio State University, College of Engineering, Gas Turbine Laboratory. 2018. Available online: <https://gtl.osu.edu/aeromechanics-research> (accessed on 24 October 2018).
31. Naval Postgraduate School. Mechanical and Aerospace Engineering—Turbopropulsion Laboratory and Gas Dynamics Laboratory. Available online: <https://my.nps.edu/web/mae/turbo> (accessed on 24 October 2018).
32. NASA Glenn Research Center. Special Projects Laboratory—Facility Description. National Aeronautics and Space Administration, 31 August 2018. Available online: <https://www1.grc.nasa.gov/historic-facilities/special-projects-laboratory/facility-description/> (accessed on 23 October 2018).
33. Schuster-Engineering GmbH. Available online: <http://schuster-sondermaschinen.de> (accessed on 25 October 2018).
34. Schenck ROTEC. Spinning Service. Available online: <https://schenck-rotec.com/services/balancing-and-spinning-service/spinning-service.html> (accessed on 25 October 2018).
35. Test Devices Inc. Available online: [www.testdevices.com](http://www.testdevices.com) (accessed on 25 October 2018).
36. Barbour Stockwell Incorporated (BSI). Available online: <http://www.barbourstockwell.com> (accessed on 25 October 2018).
37. Aerovent. Available online: <http://www.aerovent.com> (accessed on 25 October 2018).
38. Engineering, Oceanfront. Available online: <http://oceanfrontengineering.com> (accessed on 25 October 2018).
39. Lingling—Shanghai Lingling Balancing Machinery Co. Available online: <http://www.linglingbalance.com> (accessed on 25 October 2018).
40. Corporation, Piller TSC Blower. Available online: <https://www.environmental-expert.com> (accessed on 25 October 2018).
41. Element. Available online: <https://www.element.com> (accessed on 25 October 2018).
42. KTR. CLAMPEX KTR 130 and KTR 131 Data Sheet. Available online: [https://www.ktr.com/catalog/index.php?catalog=Antriebstechnik2018#page\\_284](https://www.ktr.com/catalog/index.php?catalog=Antriebstechnik2018#page_284) (accessed on 25 October 2018).
43. Mobac GmbH. Available online: [www.mobac.de](http://www.mobac.de) (accessed on 25 October 2018).
44. SKF. Available online: [www.skf.com](http://www.skf.com) (accessed on 25 October 2018).
45. Perzyna, P. Fundamental Problems in Viscoplasticity. *Adv. Appl. Mech.* **1966**, *9*, 244–368.

46. Young, J.F.; Mindess, S.; Bentur, A.; Gray, R.J. *The Science and Technology of Civil Engineering Materials*, 1st ed.; Prentice Hall: Upper Saddle River, NJ, USA, 1998.
47. Johnson, G.R.; Cook, W.H. A Constitutive Model and Data for Metals Subjected to Large Strains, High Strain Rates, and High Temperature. In *Proceedings of the 7th International Symposium on Ballistics*, Hague, The Netherlands, 19–21 April 1983; pp. 541–547.



© 2018 by the authors. Licensee MDPI, Basel, Switzerland. This article is an open access article distributed under the terms and conditions of the Creative Commons Attribution (CC BY) license (<http://creativecommons.org/licenses/by/4.0/>).